METEOROLOGICAL APPLICATIONS
Meteorol. Appl. **15**: 465–473 (2008)
Published online 13 August 2008 in Wiley InterScience
(www.interscience.wiley.com) DOI: 10.1002/met.89

The development of a shape factor instability index to guide severe weather forecasts for aviation safety

Ira Walker,* Venkatesan Chakrapani and Widad Elmahboub
Department of Mathematics, Hampton University, Hampton, VA 23668, USA

ABSTRACT: An instability index, called the shape factor (SF), for weather forecasting was proposed using temperature profiles from a NASA/LaRC-hosted web-page featuring NOAA Rapid Update Cycle (RUC) radiosonde data used for short-term weather predictions. The index of instability was predicated on the sign and magnitude of the gradient of the equivalent potential temperature. A training data set of temperature profiles was obtained for both clear and severe weather conditions and the SF index was computed. The data showed marked differences in the magnitudes of the shape factors for the two weather conditions. Calculations of SF were compared with the several well-established instability indices and there appeared marked agreement between the SF and these other metrics. It is being proposed that this new index could be used as a parameter for input to statistical weather forecasting models to enhance overall aviation safety and air traffic management efficiency. Of particular relevance is the fact that more comprehensive results can be garnered since the SF index is calculated from the entire temperature profile and not just from selected temperatures as is the case for other indices of instability. Copyright © 2008 Royal Meteorological Society

KEY WORDS atmospheric stability; thunderstorms; equivalent potential temperature

Received 24 December 2007; Revised 30 May 2008; Accepted 20 June 2008

1. Introduction

The occurrence of severe weather unfavourably impacts the capability of air traffic management systems to control the safe air travel of passengers as well as their ability to ensure the punctuality of arrival and departure flight times. A recent report issued by the Department of Transportation (OAEP, 2008) documented that in 2007 one in four flights were delayed with a significant amount being due to bad weather. Also it has been reported (Salottolo, 1994) that 41% of air traffic delays were attributable to bad weather and that this was responsible for $4.1 billion dollars in direct costs to the airline industry. Severe weather involving high amounts of rain and thunderstorms can contribute to adverse conditions such as microbursts, low visibility and unsafe runways. The formation of thunderstorms is a particularly important meteorological event that has major relevance to aviation safety. The first stage of thunderstorm formation is the ascent of large quantities of warm air due to atmospheric instability. When condensation commences, heat is released in the cloud causing it to rise forming towering cumulus clouds. Subsequently, the liquid water in the upper region of the cloud begins to fall, resulting in downdrafts. These fast moving downdrafts are responsible for inducing electrical potential in the cloud resulting in thunderstorms and possibly lightning. For the purposes of forecasting severe weather, it is useful to predict the initial stage when atmospheric instability produces significant convection (Chrysoulakis *et al*., 2003). Much effort in the aviation community has been devoted to numerical weather prediction (NWP) models to more accurately forecast severe weather. Two of the more persistent challenges have been the lack of temporal and spatial resolutions of atmospheric data and the overall unsatisfactory responsiveness of the data retrieval system to provide adequate and timely situational awareness to air traffic managers. For some time now, microwave data from remote sensing have been used to obtain information about local atmospheric conditions such as temperature profiles. Selected spectral bands from remotely sensed radiometric data can be used to approximate the temperature profile through an inversion process, whereby temperatures at selected pressure levels are processed to produce a profile with greater spatial resolution. Several multivariate regression models have been used to analyse spectroradiometric data for the inference of atmospheric temperature profiles. These include principal components regression (PCR), canonical correlation regression (CCR), maximum redundancy (MR) as well as the maximum-likelihood physics-based inversion models (Hernandez-Baquero, 2001). These temperature profiles contain valuable information that can be used to provide parameters for Model Output Statistic (MOS) products (Hughes, 2004), which give the probability of the occurrence of thunderstorms. Earlier investigations

* Correspondence to: Ira Walker, Department of Mathematics, Hampton University, Hampton, VA 23668, USA.
E-mail: ira.walker@hamptonu.edu

(Queralt *et al*., 2007) have identified different instability indices such as the potential vorticity anomaly (PV) and the Total Totals (TT) index (Miller, 1967). The former is used to monitor stratospheric intrusions into the troposphere, which directly relates to atmospheric instability. In one study (Queralt *et al*., 2007) the researchers were able to represent dynamically stable scenarios by determining if the TT index was above or below specific threshold percentiles. The study by Schmit *et al*. (2001) validated retrievals from the Geostationary Operational Environmental Satellite (GOES) using 18 infrared (IR) spectral bands to calculate profiles of temperature and moisture. Forecasters responded that these temperature profiles were very useful in producing stability indices such as Lifted Index (LI), convective available potential energy (CAPE) and the total precipitable water vapour (TPW). One of the important factors that drives local meteorological phenomena is the instability-induced vertical transport of water vapour from the Earth's surface to higher layers within the troposphere. These rising thermals containing water vapour continue to ascend until they reach the level of neutral buoyancy (LNB). Previous researchers have examined the role that instabilities play as a harbinger of impending weather conditions. In one study (Stackpole, 1967) numerical methods were implemented to calculate the pseudo-adiabatic characteristics of saturated air parcels. This process was then used to perform analyses of soundings to obtain the lifted condensation level (LCL), the level of free convection (LFC) and the convective condensation level (CCL). Stackpole (1967) devised an algorithm to be used on a high-speed computer to calculate meteorological data found on Skew T-log p graphs. The development of this mathematical-computational tool allowed the user to traverse curves of the pseudo-adiabatic lapse rate or to move from one curve to an adjacent curve to derive indices of atmospheric instability. Chrysoulakis *et al*. (2003) used data generated from the Moderate Resolution Imaging Spectroradiameter (MODIS) to assess atmospheric instability. Three well-known indices were computed based on radiosonde data and satellite derived atmospheric products, namely the K-Index (KI), the Boyden Index (BI) and (LI) (Huntrieser *et al*., 1996). In another study by Ma *et al*. (1999), the LI was calculated from entire temperature and humidity profiles which were determined from selected measured brightness temperatures by using an inversion process. Cho *et al*. (2003) conducted an experiment where measurements were obtained from an aircraft to record meteorological data to characterize stability and tropospheric turbulence. In order to formulate a complete model for weather forecasting one must account for not only the thermodynamic factors affecting atmospheric instability but the dynamical effects of wind circulation and the location of available moisture as well (Dai, 1999; Queralt *et al*., 2007). In one study (Guo *et al*., 2002), a substantial correlation was established between large moisture transports from the Bay of Bengal to the Yangtze River and the resulting amount of precipitation there. This underscores the multitude of parameters that must be incorporated into a complete model for precipitation. The current study focuses exclusively on the thermodynamic factors affecting either clear or severe weather conditions.

It is the intention of the authors to use this study as a pre-operational initiative to augment the body of knowledge pertaining to weather forecasting, particularly as applied to aviation safety. This paper proposes a method for calculating an instability metric called a Shape Factor (SF) that can be used as a metric for forecasting local weather conditions. Once the SF has become perfected as a suitable instability index it can serve as one of several inputs into a neural network computational model to more adequately warn aviation authorities of hazardous severe storms (Chauvin and Rumelhart, 1995; Venkatesan *et al*., 1997). Other possible inputs can come from vertical wind shear data (Ahrens, 1982) or from radars, lidars, surface mesonet stations, soundings and rapid scanning satellites (Wilson, 2004).

2. Data and methodology

The severity of the atmospheric instability is dependent upon the shape of the vertical gradient of the equivalent potential temperature (EPT), that is, whether sizable arc lengths of the gradient curve are negative over the entire profile. It is for this reason that the index has been called a shape factor. The data set used in this study originated from the website (http://enso.larc.nasa.gov/) hosted by NASA Langley, which contained RUC sounding meteorological profile data comprised of the local pressure in millibars, height in kilometres, absolute temperature, the absolute dew point temperature and the relative humidity. These data were extracted from targets with latitudes and longitudes that were collocated with data from the National Weather Service (NWS) at corresponding times. The NWS maintains a web-page (http://www.weather.gov/) that provides a dataset containing information about the local weather conditions and uses descriptions such as no precipitation, light rain, fog, very heavy rain and thunderstorms to give qualitative information. Data used in this analysis were for cases with either no precipitation or for severe weather with very large heavy rain, accompanied by thunderstorms. Within this report, the latter weather condition will be tagged as severe weather for the sake of brevity. The meteorological data along the vertical profile were used to calculate the EPT, which was used as the primary quantity to compute the SF index. This was done because its derivative serves an indicator of atmospheric instability, which relates to the level of saturation and precipitation in a vertical column of air. A numerical integration was performed in the direction of increasing height from the surface involving the EPT to compute the SF index. This result represents the cumulative or integrated effect of the atmospheric instability along the vertical profile. The index SF was calculated at selected geographical regions for profiles that corresponded to rain-free conditions and for conditions corresponding to severe weather. The data

DOI: 10.1002/met

show a significant difference in the SF between the data sets representing either clear or severe weather.

The data included in this study corresponded to various local times from the Middle Atlantic to the south-eastern United States. The period for the data set presented in this investigation was from September to November 2007. An assemblage of 15 data sets was constructed for both rain-free and severe weather conditions, where each data set consisted of 20 temperature soundings. Thus, there was a total of 300 temperature soundings associated with each weather condition. The authors felt that this was a large enough data set to satisfy requirements for statistical significance. An algorithm was developed to process the data by calculating the EPT and its gradient at each vertical node point and then average the results over the 20 profiles contained in each of the 15 data sets.

To calculate values of SF it was first necessary to compute the EPT, which is generally a more realistic starting point than the dry adiabatic potential temperature (PT). The former quantity allows for the presence of water vapour. As an air parcel ascends into the atmosphere it cools, which results in the formation of condensation and the gradual elimination of water vapour. Eventually, as the parcel continues to rise it will become dry and the resulting potential temperature, which remains constant, is representative of the entire process. It is this limiting value of the PT that is called the EPT and is shown in Equation (1) (Byers, 1974):

$$\theta_{\mathrm{E}} = T\left(\frac{1000}{p}\right)^{R/mC_{\mathrm{P}}} \exp\left(\frac{Lw}{C_{\mathrm{P}}T}\right) \tag{1}$$

The variable T is the absolute temperature, p is the pressure in hPa, R is the gas constant for dry air (0.287 J g^{-1}), m is the mass of the air parcel in kilograms, C_{p} is the specific heat at constant pressure (1.004 J g^{-1}. K^{-1}), w is the mixing ratio (g g^{-1}) and L (J g^{-1}) is the latent heat. The latent heat was found by using the well-known steam table for air. At each vertical location in the profile, the temperature was bounded by an upper and lower temperature in the steam table (Potter and Somerton, 1995). The latent heat, which is the change in enthalpy between the thermodynamic states of liquid and gaseous saturation, was calculated by linearly interpolating between the two latent heats at the upper and lower temperatures from the table. The specific heat was also determined by using linear interpolation from a table of published data. At each vertical location in the profile, the mixing ratio was found using Equation (2) (Byers, 1974):

$$w = 0.622\frac{rh \times e_{\mathrm{s}}}{p(100)} \tag{2}$$

In this equation, rh is the relative humidity expressed as a percentage and e_{s} is the saturation vapour pressure in hPa. The saturation vapour pressure was found using the Clasius–Clapeyron equation, which is derived in many sources on thermodynamics (Salby, 1996).

The formula for the water saturation vapour pressure for a specific temperature is then calculated as shown in Equation (3) (Salby, 1996):

$$e_{\mathrm{s}} = 1013 \times \exp\left(13.1869 - \frac{4918.7432}{T}\right) \tag{3}$$

In this formula the water vapour pressure is in hPa. Once the EPT has been calculated using Equation (1) for each vertical position in the profile a spline fit was applied to the data. The first derivative was then computed for the spline fit using a five-point differencing numerical scheme. The second derivative was also numerically calculated using central differencing. In order to determine the SF index the first derivative of the EPT at each node point was multiplied by the differential arc-length along the curve of the gradient of the EPT *versus* Z, the geopotential altitude in kilometres. The result of the integration is then normalized to remove any effects of scale and is shown in Equation (4). The non-dimensional SF index was obtained by performing the integration numerically using the trapezoidal rule from numerical analysis. This procedure was repeated for a total of 15 data sets for both weather categories, where each data set contained the average of 20 temperature soundings. A more negative value of SF is indicative of greater atmospheric instability, which is associated with the occurrence of severe weather systems. The SF index is calculated as shown in Equation (4):

$$SF = \left|\frac{1}{T_{\mathrm{F}} - T_{\mathrm{o}}}\right| \int_{Z_0}^{Z_{\mathrm{F}}} \frac{\mathrm{d}\theta_{\mathrm{E}}}{\mathrm{d}z}\sqrt{1 + (\alpha\beta\frac{\mathrm{d}^2\theta_{\mathrm{E}}}{\mathrm{d}z^2})^2}\mathrm{d}z \tag{4}$$

where T_{F} and T_0 are the absolute temperatures at the highest point in the profile and at the surface of the Earth, respectively, α and β are scaling factors shown in Equations (5) and (6), respectively, and θ_{E} is the EPT.

$$\alpha = Z_{\mathrm{F}} - Z_0 \tag{5}$$

$$\beta = \frac{Z_{\mathrm{F}} - Z_0}{T_{\mathrm{F}} - T_0} \tag{6}$$

The product of α and β multiplied by the second derivative of the EPT in Equation (4) non-dimensionalizes the expression beneath the radical sign.

The findings from this study were compared with the metric KI, which is a well established index for instability (George, 1960). The calculation of KI measures the thunderstorm potential as a function of the vertical temperature lapse rate at a temperature corresponding to a pressure of 850 hPa, and a temperature at 500 hPa, the dew point absolute temperature corresponding to a low level moisture content at 850 hPa and the depth of the moist layer at 700 hPa. The formula for KI is shown in Equation (7):

$$KI = (T^{850} - T^{500}) + T_{\mathrm{d}}{}^{850} - (T^{700} - T_{\mathrm{d}}{}^{700}) \tag{7}$$

DOI: 10.1002/met

Table I. Relation between K-Index and thunderstorm potential.

K-Index	Thunderstorm potential
0–15	0%
16–19	20% unlikely
20–25	35% isolated thunderstorm
26–29	50% widely scattered thunderstorms
30–35	85% numerous thunderstorms
>36	100% chance for thunderstorms

The range for KI corresponding to the probability of thunderstorms is represented in Table I (Chrysoulakis *et al*., 2003).

The literature is replete with instability indices that various researchers have developed with some measure of success (Showalter, 1953; Galway, 1956; Rackliff, 1962; Boyden, 1963). In some studies, intercomparisons were made between the various instability indices (Michalopoulou and Jacovides, 1987; Dalezios and Papamanolis, 1991). However, one unsolved challenge is that the reliability of these various instability indices is linked to geographical region and season. It would be helpful if an instability index could be developed with universal applicability.

Another commonly used indicator of convective instability is the BI (Boyden, 1963), which is defined as shown in Equation (8):

$$BI = Z^{700-1000} - T^{700} - 200 \tag{8}$$

where, Z is the difference in geopotential height between the two atmospheric layers at 700 hPa and at 1000 hPa in decametres, T^{700} is the atmospheric temperature at 700 hPa in°C, and 200 is the constant subtracted to scale the index to be within a conventionally accepted range (Boyden, 1963). For the BI the threshold value indicative of severe weather activity is 94, where values greater than this benchmark suggest the presence of thunderstorms (Chrysoulakis *et al*., 2003).

An instability metric which has demonstrated a high degree of success is the Total Totals (TT) index as described by Huntrieser *et al*. (1996), and which is defined as shown in Equation (9):

$$TT = 2(T^{850} - T^{500}) - T^{850} + {T_\mathrm{d}}^{850} \tag{9}$$

This index uses the atmospheric absolute temperature difference between the layers at 850 hPa and at 500 hPa along with the absolute temperature corresponding to 850 hPa and the dew point absolute temperature at 850 hPa. The thunderstorm threshold for TT varies from 45 to 50, which is geographically and seasonally dependent as was demonstrated by Marinaki *et al*. (2006). Higher values for TT are associated with a greater probability of thunderstorms.

The final instability index that was used to compare with the SF was the Humidity Index (HI) (Equation (10)):

$$HI = (T^{850} - {T_\mathrm{d}}^{850}) + (T^{700} - {T_\mathrm{d}}^{700}) + (T^{500} - {T_\mathrm{d}}^{500}) \tag{10}$$

The value of HI depends on the differences between the atmospheric temperature and dew point temperature for pressure levels corresponding to 850, 700 and 500 hPa and was described with added detail by Huntrieser *et al*. (1996). There exist many more indices for weather forecasting that have been widely investigated and described in the meteorological literature (Bidner, 1970; Andersson *et al*., 1989; Collier, 1994). The most important objective is to classify and ultimately rank the many indices regarding their applicability to various geographical and seasonal domains. This database would be invaluable to the many users of weather forecasting information, including the members of the aviation industry.

Another approach to weather forecasting is to understand the dynamics associated with convective instability by examining the differential equation that governs the ascent and descent of air parcels in the troposphere. If thermal stability exists, then the air parcel will be displaced vertically upward, but then will cool as it ascends, causing it to ultimately descend. After it descends for a certain distance its temperature will increase, which will cause it to rise again. The motion of the air parcel under thermal stability will behave as a harmonic oscillator that is displaced periodically at a frequency equal to its natural frequency. This is contrasted with thermal instability which is characterized by the continuous vertical displacement of air parcels because of their buoyancy due to lower densities and higher temperatures relative to the ambient lapse rate of 1 °C *per* 100 m. If a large volume of moist unstable air is perturbed by disturbances in the wind field, a convective current will be initiated, which establishes the conditions for precipitation. After condensation has begun, latent heat is released which increases the amount of buoyancy (Batten, 1984). It is common practice to model the physics of rising thermals as a second order system with a restoring force simulating a spring in accordance with Hooke's Law (Salby, 1996). The governing differential equation is shown in Equation (11):

$$\frac{\mathrm{d}^2 z'}{\mathrm{d}t^2} + N^2 z' = 0 \tag{11}$$

where z' is the displacement of the air parcel about an equilibrium position and N^2 is the square of the natural frequency of oscillation. The parameter N is called the Brunt–Väisäillä Frequency (BVF) that reflects the 'stiffness' of the buoyancy spring. Values of $N^2 > 0$ are directly proportional to the 'stiffness' of the buoyancy spring, signifying that the rising thermals are characterized by stability. The formula for calculating N^2 is shown in Equation (12) (Salby, 1996):

$$N^2 = g\frac{\mathrm{d}\ln\theta}{\mathrm{d}z} \tag{12}$$

DOI: 10.1002/met

The constant g is the acceleration due to gravity, i.e. 0.0098 km s^{-2}. This square of the BVF was computed in this study and subsequently used as a parameter to validate the reliability of the SF. The solution to Equation (11) contains sinusoidal terms that give way to oscillations. For the case where $N^2 < 0$, the resulting solution contains a linear combination of exponential terms that theoretically amplify unbounded as the time increases and is shown in Equation (13) and can be derived from any fundamental book of Ordinary Differential Equations (Nagle and Saff, 1993; Zill, 2000). For small displacements of air parcels they tend to grow, even overcoming the retarding effects of friction between adjacent layers:

$$z' = Ae^{Nt} + Be^{-Nt} \tag{13}$$

From this equation it can be clearly seen that as t increases, the leftmost exponential term dominates and grows unbounded. The magnitude and particularly the sign of N^2 can therefore be used as some measure of thermal stability.

3. Results and discussion

Figure 1 shows the profiles of EPT for both weather categories. Since a negative gradient is indicative of thermal instability, both weather categories demonstrate some pre-convective activity. However, the more negative gradient is shown for the cases when severe weather activity occurred. The data show the marked drop near 5 km, which would accounted for the more negative value of SF since it represents an integrated effect over the entire profile. Figure 2 shows the profiles of the mixing ratio for water vapour. As expected, the data show the presence of significantly higher concentrations of water vapour below a height of 6 km. These results indicate that at the times of the recorded data, the water vapour had not yet precipitated out of the atmosphere. The values of SF as described above represent mathematically the line integral of the gradient of the EPT along the curve itself. Therefore, preliminary results suggest that SF can be used as a benchmark indicator of local weather conditions.

The typical temperature profiles for both weather conditions considered in this study are shown in Figure 3. Notice that the temperature values in the case for severe weather are slightly higher at several altitude locations in the profile. This is due to the release of sensible heat associated with the condensation of water vapour.

Three examples showing the profiles for the moisture level depths (MLD) for both weather conditions are displayed in Figure 4. The MLD is the difference between the temperature and the dew point temperature. The dew point temperature is the temperature of the air parcel for a specific air pressure at which condensation commences. The smaller the MLD the closer the air parcel is to becoming saturated, and the closer the atmosphere is to being unstable, initiating the conditions for weather with precipitation. Other important factors contributing to

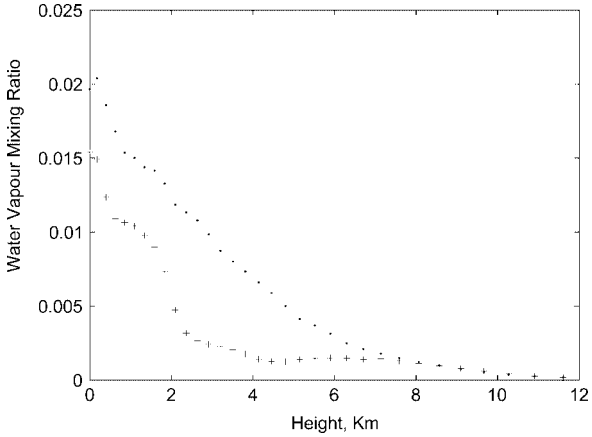

Figure 2. Water vapour mixing ratio (g g^{-1}) *versus* geopotential altitude (km) for rain-free weather (plus signs) and a highly convective event with severe weather activity (dots).

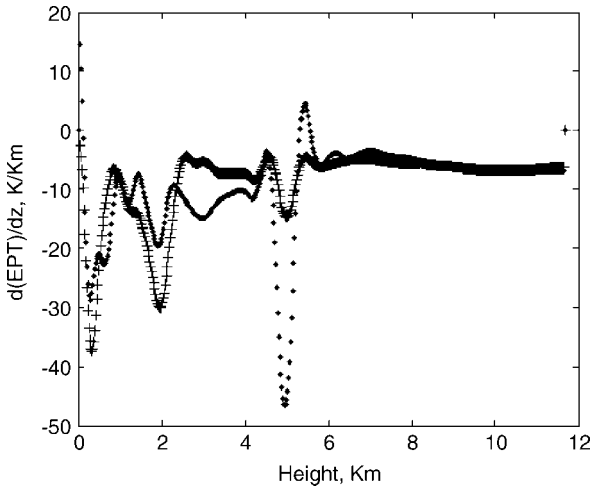

Figure 1. Vertical gradient of EPT (K km^{-1}) *versus* geopotential altitude (km) for rain-free weather (plus signs) and a highly convective event with severe weather activity (dots).

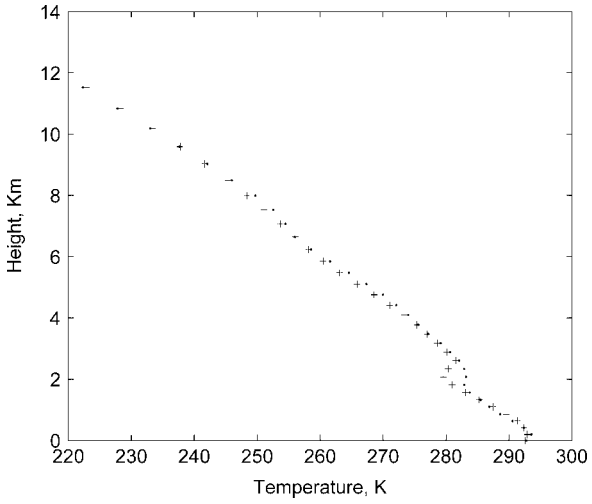

Figure 3. Typical tropospheric temperature (K) *versus* geopotential altitude (km) for rain-free weather (plus signs) and a highly convective event with severe weather activity (dots).

DOI: 10.1002/met

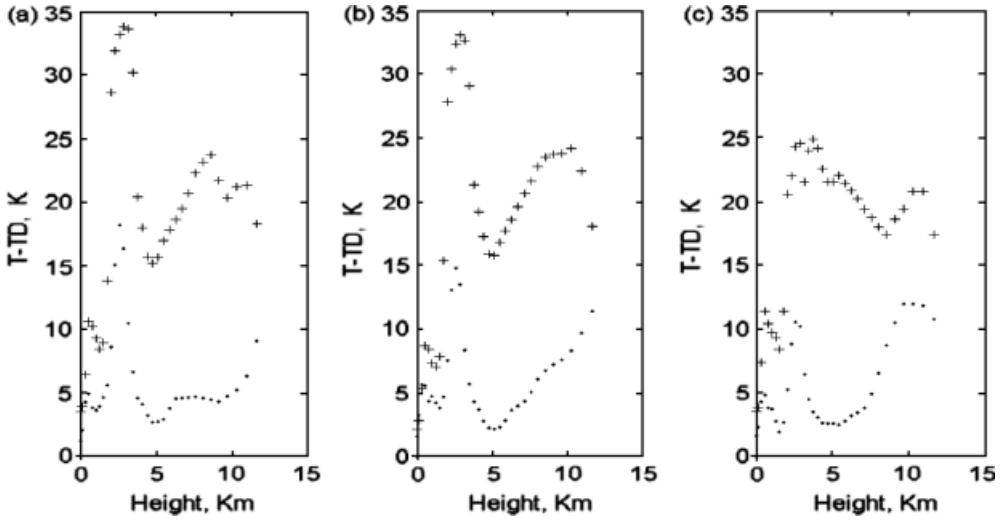

Figure 4. (a)–(c)Three typical profiles of moisture level depth (K) *versus* geopotential altitude (km) for rain-free weather conditions (plus signs) and highly convective events with severe weather (dots).

instability include the lapse rate and the vertical structure of moisture.

One notable and consistent feature shown in Figure 4 is that the lowest value of MLD for the case of severe weather occurs at an altitude near 5 km, which is the same altitude associated with the prominent negative value of the gradient of the equivalent potential temperature as shown in Figure 1. Another interesting characteristic of the data is the appearance of two distinguishable peaks of the MLD for the case of no rain. The reason for this phenomenon is unclear to the authors.

Calculations of SF used temperature profiles from weather reporting stations in the Mid-Atlantic and southeast Atlantic coast of the United States. The weather and time were determined by obtaining information from the NWS. In order to define the training set (a set of data to determine SF values critical for the occurrence of severe weather) for this methodology, values of SF were computed only for conditions that were either completely rain-free (neither fog nor light rain) and for cases when there was severe weather. The sample consisted of 15 datasets, each with an average of 20 profiles and the SF was computed based on the averages of the first and second derivatives of EPT using Equation (5). The data for both weather conditions were accumulated and plotted in the form of histograms. These plots are shown in Figures 5 and 6. The data demonstrated a marked difference between the data corresponding to no precipitation and the data that was for severe weather conditions. For the case of clear weather, there was a peak centred on an SF of −20. For the heavy precipitation data the peak occurred at −40 and another less prominent peak at −120. A threshold value distinguishing the two opposite weather conditions was at an SF of −30. These results suggest that SF can be used as predictor of severe weather with thunderstorms.

Based on the information displayed in Figures 5 and 6, the thresholds of SF for clear weather and severe weather were for values that were greater than or equal

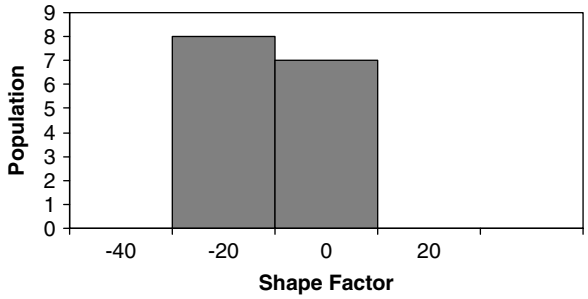

Figure 5. Distribution of shape factor calculations for rain-free weather. Histogram results are based on 15 datasets, where each dataset contained an average of 20 temperature profiles.

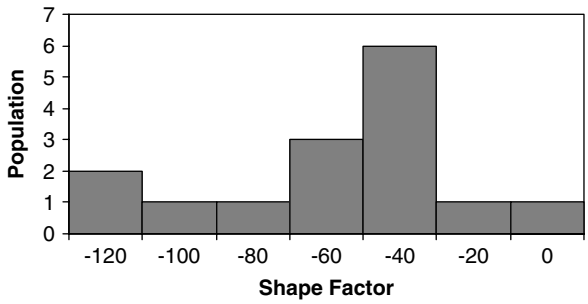

Figure 6. Distribution of shape factor calculations for severe weather. Histogram results are based on 15 datasets, where each dataset contained an average of 20 temperature profiles.

to −30 and less than −30, respectively. The average and standard deviation for the case of no rain were −11.2586 and 7.702, respectively. For the case of severe weather, the average was −57.5742 and the standard deviation was 32.645. Although it would be advantageous if the standard deviations could have been smaller with greater sample sizes, this study was intended to be exploratory and the results from this investigation can assuredly lay the foundation for further studies. Nevertheless, these results still have significant merit since they definitely

DOI: 10.1002/met

establish a clear and decisive threshold for identifying temperature profiles that correlated well with either clear or severe weather. For the case of clear weather, the next to the last data entry for SF in Table III indicates one value which is inconsistent with the other results. Presently, the reason for this aberrant value for SF is unknown.

Each value of SF shown in Table II represents an average that was computed for the severe weather category using 20 temperature profiles. Comparisons were made between the values of SF with several conventional instability indices using corresponding data. Similar data are shown in Table III for the category of weather marked by no precipitation. The calculations of the different indices in each row of both tables corresponded to the identical dataset.

The data for both weather categories show overall agreement between the results based on SF values compared with the KI. For nearly every instance that the SF predicted either clear weather or severe weather the computed value for KI rendered the same result. Future research may provide more reliable population distributions of SF so that statistical forecasting can be obtained with further refinement of the training datasets for clear and severe weather conditions.

Table II. Comparison between shape factor and various instability indices for severe weather.

SF	KI	TT	BI	HI
−49.5	32.2	43.6	97.7	21.0
−36.2	27.4	40.8	95.0	22.4
−38.5	11.9	32.5	94.4	37.0
−59.0	29.5	46.2	95.4	20.1
−48.0	26.0	43.4	95.5	17.1
−65.8	25.5	42.1	95.2	20.5
−30.1	33.0	44.1	96.4	15.4
−19.3	30.0	43.2	98.0	21.2
−2.4	18.6	44.0	94.7	32.8
−71.1	33.8	44.8	96.0	11.1
−63.3	31.6	45.8	94.9	8.4
−112.5	32.8	44.6	94.6	5.4
−49.7	33.2	46.0	96.1	11.1
−106.0	32.7	45.0	95.3	4.8
−112.1	32.9	44.0	94.7	4.5

Table III. Comparison between shape factor and various instability indices for clear weather.

SF	KI	TT	BI	HI
−21.3	2.2	33.2	93.5	52.3
−21.3	14.1	39.5	92.8	29.9
−13.1	13.2	35.8	94.8	39.6
−18.2	15.1	39.8	95.1	43.6
−15.4	5.8	36.3	92.4	43.1
−2.0	−13.5	24.7	92.2	71.3
−8.9	−3.4	31.9	90.6	51.0
−17.8	14.6	34.4	94.2	36.5
−18.6	5.4	32.2	93.3	45.8
−12.6	11.5	38.9	94.5	39.5
−9.3	12.7	39.8	93.2	31.4
−2.3	−5.9	26.0	92.9	66.3
−5.1	−10.9	22.8	91.9	64.3
4.1	−5.8	24.7	90.2	52.3
−7.2	−11.3	25.3	92.2	70.9

The TT index also compared well with SF for both categories of weather. Generally, values of TT greater than or equal to 40 were indicative of thunderstorms or high convective instability. Marinaki *et al.* (2006) investigated the TT index for various regions in Greece during the time period from April to October. Their radiosonde data were obtained from observations made during the period from 1981 to 2003 and indicated that values of TT greater than or equal to 45 corresponded to thunderstorms.

General agreement is also seen from comparisons between SF and the values of BI. Thunderstorm activity was indicated by values of BI that were greater than or equal to 95 (Marinaki *et al.*, 2006). In that same study the BI was fairly constant over all four seasons. The reliability of the BI to predict thunderstorms is well established, which helps to validate the SF.

The last index that was used for comparison was HI. This index generally demonstrated the same degree of consistency as was exhibited by the other indices, including the SF. However, the HI might be more sensitive to both geographical and seasonal domains. An earlier study (Marinaki *et al.*, 2006) showed that HI indicated marked variability for a given weather category over a 3-month period. Other indices in that same study were more consistent with regards to weather category.

The square of the Brunt–Väisäillä Frequency, N^2, was calculated for both weather conditions investigated in this study using Equation (10). Figure 7 shows the profiles of this parameter for six typical soundings, where three were for rain-free weather conditions and the other three were for weather conditions marked by severe weather. A large negative spike was exhibited for all three soundings corresponding to highly convective activity. These results were compared with calculated values of SF for further validation of this new instability index. Using the same data shown in Figure 7(a), the calculated values of SF for the cases of rain-free weather and severe weather were −21.2925 and −105.95 respectively. For the data shown in Figure 7(b) these same values for SF were −15.3638 and −65.7823. Finally, for the data shown in Figure 7(c), these same calculated values for SF were −2.2940 and −36.1958. These results indicate that the SF index demonstrates good agreement with N^2 as a marker for highly convective weather systems. It is noteworthy that for the severe weather condition the large negative spike in the Brunt–Väisäillä Frequency occurs around 5 km, which is indicative of instability. This corresponded to roughly the same altitude where the MDL was the lowest for the severe weather data as shown in Figure 4. Another important trend is that there appears to be a direct correlation between the

DOI: 10.1002/met

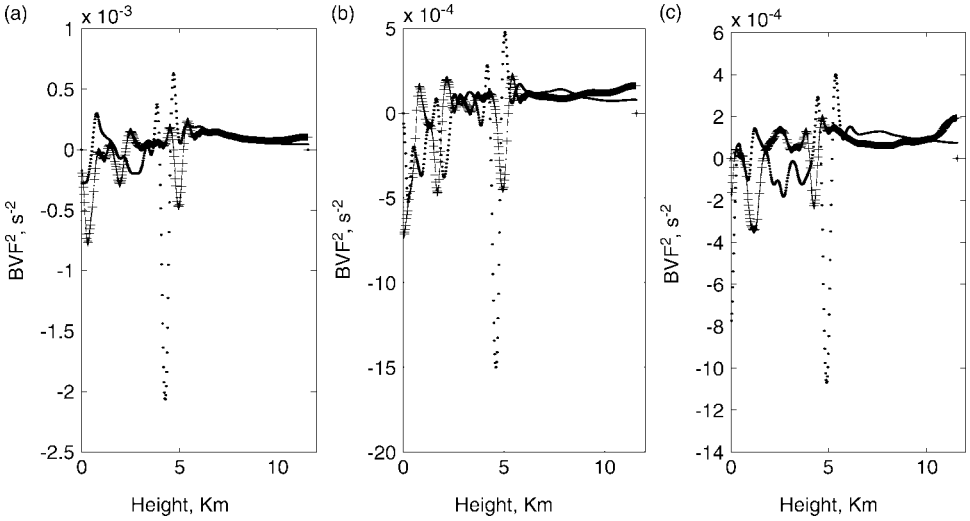

Figure 7. (a)–(c) Three typical profiles of the Brunt–Väisäillä Frequency squared (K s^{-2}) *versus* geopotential altitude (km) for rain-free weather conditions (plus signs) and highly convective events with severe weather (dots).

level of the negative spike for N^2 and the SF. When the SF was the most negative (-105.95) the value of N^2 was -2.1×10^{-3}. For SF values of -65.7823 and -36.1958 the values for N^2 were -1.5×10^{-3} and -1.1×10^{-3}, respectively. For the rain-free weather data in Figure 7, the preponderance of the values for N^2 were positive, even though in Figure 7(a) the most negative value for clear weather is -0.75×10^{-3}. The data for severe weather even exhibits values for N^2 that are positive for certain intervals of altitude. Although the well-established stability indices and the Brunt–Väisäillä Frequency are good indicators of weather conditions, the SF demonstrates greater sensitivity to minute variations of the temperature profile. It is for this reason that once this methodology has been refined it holds the potential of being highly discriminatory with respect to distinguishing different classes of weather conditions. Eventually, a large enough training set can be generated so that a meteorological model can be developed to not only determine clear and stormy weather, but also for gradations of weather between these two extremes.

4. Conclusions and future plans

The results from this study suggest that the SF index can be used as a predictor of adverse impending weather conditions. One advantage to this approach is that the SF provides a more comprehensive index since it is based on the entire temperature profile and not on just selected portions as is the case for some indices. This index is predicated on pre-convective weather systems being characterized by a negative gradient of the EPT. A total of 15 average values of SF were calculated over 20 temperature profiles for both clear and severe weather conditions. Comparisons between the SF and well-established instability indices demonstrated significant similarity in their usefulness as indicators of thermal instability in the atmosphere. Favourable comparisons were also obtained with the Brunt–Väisäillä Frequency and the MLD. These results further demonstrated the applicability of the SF index as a potential parameter for input to statistical models to forecast weather. The next task is to apply this methodology to temperature profiles over successive days to acquire a time series of the SF values to discern any trends for reliably forecasting of severe weather. As has already stated, in this study a total of 20 profiles were used to compute the values of SF. A desirable data product would be a statistical model that would permit forecasting with fewer profiles. This would greatly reduce the analysis time, which is desirable for improving aviation related weather forecasting. Including a stability parameter in physical and/or statistical modelling can improve local severe storm predictions. This work will be extended to develop new algorithms to fit the data into appropriate statistical distribution to enable us to construct stochastic and numerical models such as neural networks. These models will then be used to produce more accurate forecasts of the local weather at shorter time scales (1–24 h). This will in turn enable us to warn the public and local authorities so that they will have greater situational awareness and are able to make more timely decisions. Finally, because the results presented in this study were for the eastern and south-eastern United States, more analysis needs to be done over different geographical and seasonal domains to obtain a more generalized index.

References

Ahrens CD. 1982. *Meteorology Today: An Introduction to Weather, Climate and the Environment*, 4th edn. West Publishing Company: St. Paul, MN; 413.

Andersson T, Andersson M, Jacobsson C, Nilsson S. 1989. Thermodynamic indices for forecasting thunderstorms in southern Sweden. *Meteorological Magazine* **116**: 141–146.

Batten LJ. 1984. *Fundamentals of Meteorology*, 2nd edn. Prentice Hall, Inc.: Englewood Cliffs, NJ; 55.

Bidner A. 1970. The air force global weather central severe weather threat (SWEAT) index- a preliminary report. *Air Weather Service Aerospace Review* **70**(3): 2–5, AWS RP 105-2.

DOI: 10.1002/met

Boyden CJ. 1963. A simple instability index for use as a synoptic parameter. *Meteorology Magazine* **92**: 198–210.
Byers H. 1974. *General Meteorology*, 4th edn. McGraw-Hill: New York, NY; 119.
Chauvin Y, Rumelhart DE. 1995. *Backpropagation: Theory and Architectures and Applications*. Lawrence Erlbaum Associates: Boca Raton, FL; 561.
Cho JY, Newell RE, Anderson BE, Barrick JD, Thornhill KL. 2003. Characterization of tropospheric turbulence and stability layers from aircraft observations. *Journal of Geophysical Research* **108**: D208784, DOI:10.1029/2002JD002820.
Chrysoulakis N, Spiliotopoulos M, Domenikiotis C, Dalezios N. 2003. Towards monitoring of regional atmospheric instability through MODIS/AQUA images. *Proceedings of the International Symposium*, Volos, 7–9 November 2003.
Collier CG. 1994. Forecasting thunderstorm initiation in north-west Europe using thermodynamic indices, satellite and radar data. *Meteorological Applications* **1**: 74–84.
Dai AG. 1999. Recent changes in the diurnal cycle of precipitation over the United States. *Geophysical Research Letters* **26**: 341–344.
Dalezios NR, Papamanolis NK. 1991. Objective assessment of instability indices for operational forecasting in Greece. *Meteorology and Atmospheric Physics* **45**: 87–100.
Galway JG. 1956. The lifted index as a predictor of latent instability. *Bulletin of the American Meteorological Society* **37**: 528–529.
George JJ. 1960. *Weather Forecasting for Aeronautics*. Academic Press: New York; 409–415.
Guo Y, Zhao Y, Wang J. 2002. Numerical simulation of the relationship between the 1998 Yangtze River valley flood and SST anomalies. *Advances in Atmospheric Sciences* **19**: 391–404.
Hernandez-Baquero E. 2001. Comparison of statistical inversion techniques for atmospheric soundings. *Geoscience and Remote Sensing Symposium. 2001. IGARSS 2001. IEEE 2001 International* **4**: 1705–1707.
Hughes KK. 2004. Probabilistic lightning forecast guidance for aviation. *11th Conference on Aviation, Range and Aerospace*, Hyannis, 4–8 October 2004.
Huntrieser H, Schiesser H, Schmid W, Waldvogel A. 1996. Comparison of traditional and newly developed thunderstorm indices for Switzerland. *Weather and Forecasting* **12**: 108–125.
Ma XL, Schmidt TJ, Smith WL. 1999. A nonlinear physical retrieval algorithm- its application to the GOES-9/9 sounder. *Journal of Applied Meteorology* **38**: 501–513.
Marinaki A, Spiliotopoulos M, Michalopoulou H. 2006. Evaluation of atmospheric instability indices in Greece. *Advances in Geosciences* **7**: 131–135.
Michalopoulou H, Jacovides C. 1987. Instability indices for the Cyprus area. *Meteorology and Atmospheric Physics* **37**: 152–158.
Miller RC. 1967. Notes on analysis and severe storm forecasting procedures of the military, Weather Warning Centre, Tech. Rep. 200, AWS, U.S. Air Force: 94.
Nagle RK, Saff EK. 1993. *Fundamentals of Differential Equations*, 3rd edn. Addison-Wesley Publishing Co.: Reading, MA; 200.
Office of Aviation Enforcement and Proceedings (OAEP). 2008. Air Traffic Consumer Report, Department of Transportation, 14–23.
Potter M, Somerton C. 1995. *Thermodynamics for Engineers*. McGraw-Hill: New York; 297.
Queralt S, Hernandez E, Gallego D, Iturrioz I. 2007. Atmospheric instability analysis and its relationship to precipitation patterns over the western peninsula. *Advances in Geosciences* **10**: 39–44.
Rackliff P. 1962. Application of an instability index to regional forecasting. *Meteorology Magazine* **91**: 113–120.
Salby M. 1996. *Fundamentals of Atmospheric Physics*, 1st edn. Academic Press, Inc.: San Diego, CA; 112.
Salottolo G. 1994. *Oral Presentation to the National Aviation Weather Service Committee at the National Academy of Sciences*: Washington, DC, 1 September 1994.
Schmit TJ, Feltz WF, Menzel WP, Jung J, Noel AP, Heil JN, Nelson JP, Wade GS. 2001. Validation and use of GOES sounder moisture information. *Weather and Forecasting* **17**: 139–154.
Showalter AK. 1953. A stability index for thunderstorm forecasting. *Bulletin of the American Meteorological Society* **34**: 250–252.
Stackpole JD. 1967. Numerical analysis of atmospheric soundings. *Journal of Applied Meteorology* **6**: 464–467.
Venkatesan C, Raskar SD, Tambe SS, Kulkarne BD, Keshavamurty RN. 1997. Prediction of all Indian summer monsoon rainfall using error-backpropagation neural networks. *Meteorology and Atmospheric Physics* **62**: 225–240.
Wilson JW. 2004. Thunderstorm initiation and evolution using IHOP: implications for aviation weather nowcasting. *11th Conference on Aviation, Range and Aerospace*, Hyannis, October 4–8, 2004.
Zill DG. 2000. *A First Course in Differential Equations*, 5th edn. Brooks/Cole a division of Thomson Learning: Pacific Grove, CA; 192.

DOI: 10.1002/met